

Scaling and Multiscaling: Fractals and Multifractals

Leo P. Kadanoff

The Research Institutes, University of Chicago, Chicago, Illinois 6061.5, U.S.A.

(Received March 16, 1991)

Many different physical situations can be described by multifractal distributions. A general framework is presented. Several specific examples are discussed.

I. INTRODUCTION: SAMPLE SCALING

For many years, we have been used to describing physical situations in terms of a scaling analysis. Scaling is a variant of dimensional analysis in which we argue that there is a characteristic size or scale by which we can set the order of magnitude of things of interest. Hydrodynamics gives us many simple examples such scaling analysis.

I-1. Blasius profile

Consider for example the Blasius analysis of flow past a flat plate. In this situation, see Fig. 1.1, a stream of fluid is flowing past a semi-infinite flat plate. The basic equations to describe this situation are the Navier Stokes equations:

$$\mathbf{u}_t + \mathbf{u} \cdot \nabla \mathbf{u} = -(\nabla p)/\rho + \nu \nabla^2 \mathbf{u} \quad (1.1)$$

Here \mathbf{u} is the fluid velocity, p the pressure, ρ the density and ν the kinematic viscosity. This statement is $F = ma$, applied to the fluid mass with forces from pressure and viscous drag. The second of our equations is the condition for the conservation of mass in this fluid, which assumes that the fluid is incompressible. It is

$$\nabla \cdot \mathbf{u} = 0 \quad (1.2)$$

We employ the usual boundary conditions, namely that $\mathbf{u} = 0$ on solid boundary. In our particular problem we that the flow be steady and the U goes to a constant, $(U,0)$ as y goes to \pm infinity. We consider the flow to be two dimensional and completely neglect the third direction.

To see the structure of the result take the curl of Eq. (1.1) to find

$$(\mathbf{u} \cdot \nabla) \nabla \times \mathbf{u} = \nu \nabla^2 \nabla \times \mathbf{u} \quad (1.3)$$

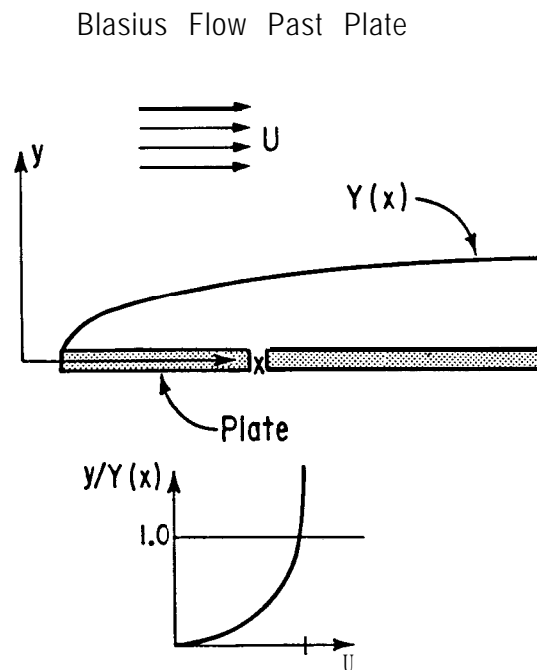


FIG. 1.1. Blasius Figure. This figure shows first the geometry of the situation described by Blasius and then the form of the velocity profile achieved.

The Blasius solution is based upon the idea that there is a characteristic scale of the y coordinate, which varies with x , the distance along the plate measured from its beginning. Therefore, every function of y will depend upon y in the form of functions of $y/Y(x)$ where $Y(x)$ is the characteristic scale of y . The scale of x is simply the distance from the leading edge of the plate. We look far downstream, where the scale of Y is much smaller than the scale of x . In this limit, one can neglect the $(\partial/\partial x)^2$ term in ∇^2 in comparison with the $(\partial/\partial y)^2$ term. Thence (1.3) reduces to

$$(u \cdot \nabla) \nabla \times u = \nu \frac{\partial^2}{\partial y^2} \nabla \times u \quad (1.4)$$

To an order of magnitude one can estimate the size of a y -derivative as being proportional to $Y(x)^{-1}$, while an x derivative is of the order of the inverse x -scale x^{-1} . A typical value of u_x is just U . Thus, if the two terms in Eq. (1.4) are to balance out, we must have that, to an order of magnitude:

$$U/x \sim \nu/Y(x)^2 \quad (1.5)$$

so that the y scale is

$$Y(x) = (\nu x/U)^{1/2} \quad (1.6)$$

Using this idea, one can in fact, construct a solution of (1.4) assuming that the x-component of the velocity has the form

$$u_x = U\Psi'(y/Y(x))$$

Then, the continuity equation, Eq. (1.2) provides a solution for the y-component of the velocity, namely

$$u_y = -UY'(x)[\Psi(\eta) - \eta\Psi'(\eta)], \eta = y/Y(x)$$

One then uses Eq. (1.4) to write down an ordinary differential equation for Ψ ,

$$-\frac{\partial}{\partial \eta}(\Psi\Psi'') = 2\frac{\partial^4}{\partial^4 \eta}\Psi$$

which can be solved numerically.

The physical idea upon which this is all based is that the flow is the same for all x except for the change of scale, represented by the Y(x). Notice that the answer can be represented by simple power laws, for example that Y(x) is proportional to $x^{1/2}$. We see here that the simple power laws are an outcome of the idea that as one goes to larger x nothing changes except the scale of y.

1-2. Widom scaling*

A second example is provided by the **Widom** analysis of simple scaling behavior in critical phenomena. Consider a magnet near its critical point. There are three quantities of interest to us. **Two** of these measure the deviations from the critical point: a dimensionless magnetic field $h = \mu H/k T$ and a dimensionless measure of the deviation of the temperature, T, from its critical value, T_c . This second dimensionless quantity is then $t = T - T_c/T_c$. Near the critical point both of these are much smaller than unity. The statement of scaling is that the powers of the temperature deviation provide a characteristic scale of all physical quantities. For example, the magnetic field always appears in the theory in the combination h/t^Δ , where Δ is the critical index for the magnetic field. Correspondingly, the magnetization appears in the combination m/t^β , with β being another critical index. The content of this statement is then that the magnetization appears in the scaling form:

$$m(h, t) = t^\beta m^* \left(\frac{h}{t^\Delta} \right) \quad (1.7)$$

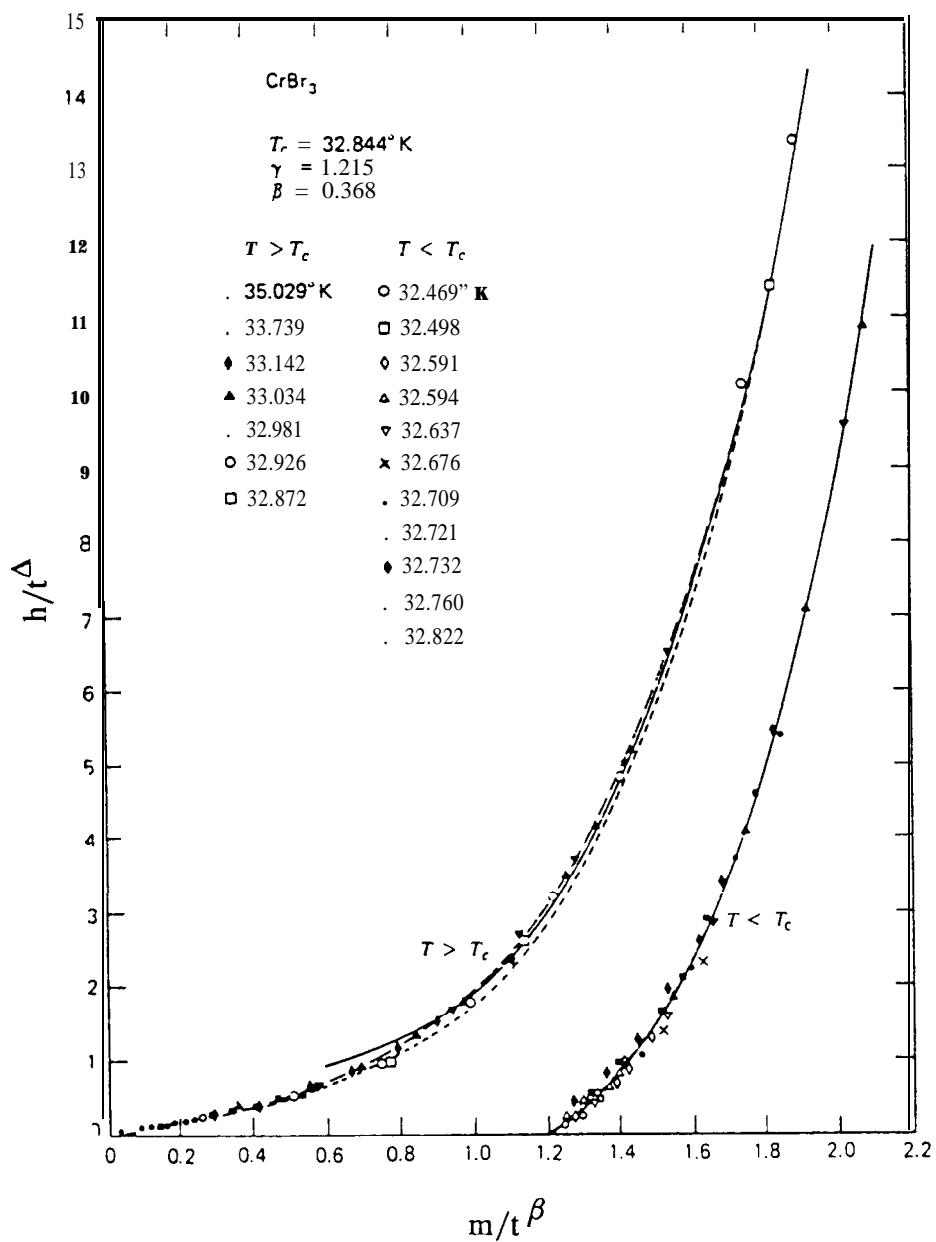


FIG. 1.2. Experimental Data for scaled magnetic field versus scaled magnetization. The experiment was done by T.J. Ho and J.D. Litster, Phys. Rev. Letts 22, 603(1969). The fact that all the data fits on two curves (one for $T > T_c$, the other for $T < T_c$) shows that this systems obeys the Widom scaling hypothesis. (The figure is drawn from Balescu, ref 1).

If h is of the same order of magnitude as t^Δ then m^* is of order one and m is of order t^β . One can check a statement like (1.3) experimentally. One takes data on m as a function of h and t . One then guesses values for β and A . Then one plots $m(h,t)/t^\beta$ on one axis and h/t^Δ on the other. If β and A have been correctly chosen, then all the data for different values of t should fall on a single curve. One adjusts the parameters to make this happen as closely as possible. Fig. (1.2) shows the results of one such fitting. Notice that it really does work.

I-3. Kolmogorov theory of turbulence²

Our third example is drawn from the Kolmogorov theory of turbulence. Imagine that one measures the velocity of fluid in a sensor moving rapidly through a turbulent fluid. The fluid is described by a Reynolds number $R = UL/\nu$ which is large. In this Reynolds number U is a typical relative velocity of the flow, L is a typical length scale and ν is the kinematic viscosity of the fluid. Now consider the Fourier transform of the velocity signal

$$V(\omega) = \int_0^T dt v(t) e^{i\omega t} \quad (1.8)$$

and form $P(\omega)$ the squared magnitude of Fourier Transform

$$P(\omega) \sim |V(\omega)|^2 \quad (1.9)$$

This $P(\omega)$ is called the power spectrum. According to the Kolmogorov theory there is a characteristic dissipative frequency $\omega_D \sim (U/L) R^{1/4}$ which scales as a power of the Reynolds number and all other frequencies are to be compared with that one. The result is that there is a scaling form for the power spectrum. Kolmogorov also predicted the values of the scaling indices and ended up with a answer in the form

$$P(\omega) \sim \omega^{-5/3} \times p^*(\omega/\omega_D) \quad (1.10)$$

with the x in ω_D being $1/4$. In Fig. 1.3, this theoretical result is compared with experiment. Once again the fit is good.

The argument for the Kolmogorov theory arises from the analysis of the Navier Stokes equation. One looks at the density of kinetic energy $|u(r,t)|^2/2$ and notices that it obeys an equation of the form

$$\frac{\partial}{\partial t} |u(r,t)|^2/2 + F = -D \quad (1.11)$$

here the dissipation term is

$$D = \nu |\nabla u|^2$$

and represents a loss of kinetic energy to heat. The flux term is

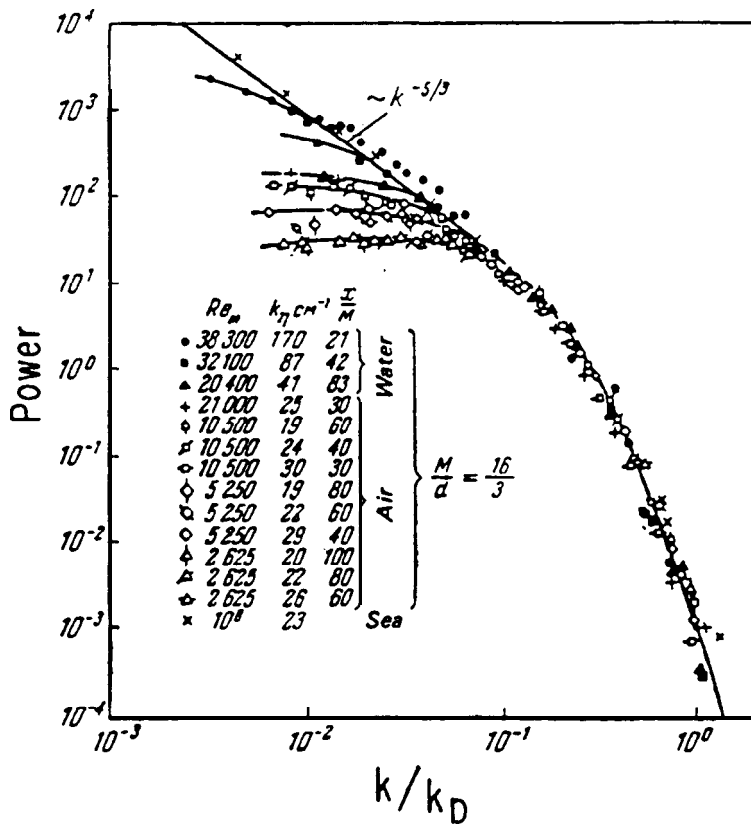


FIG. 1.3. Power spectrum, Kolmogorov theory compared with experiment. The figure is drawn from Monin and Yaglom (reference 2) Volume 2, Figure 75. The theoretical prediction is that all the data fall on a single curve, which has on the left-hand end a straight line portion with slope $-5/3$. The fit is excellent. The data falls off the curve on the left-hand side because the fluctuations are limited by the finite size of the container.

$$F = u \cdot (u \cdot \nabla) u - \nu \nabla^2 |u|^2 \quad (1.12)$$

and represents the effect of moving energy up and back between different wave number components. In fact, one visualizes putting in energy at long wavelengths and seeing it cascade down into shorter and shorter wavelengths. Let u_k be the typical velocity which the system has in wave vectors (inverse wavelengths) of order k . Then, at the longer wavelengths (for which the dissipation is very small) the flux on scale k is of the order

$$F \sim k u_k^3 = \varepsilon_k \quad (1.13)$$

Kolmogorov argument is that ε_k must be independent of k in this longer wavelength region since

the flux moves energy from scale to scale and it cannot be lost. Thus, the flux is independent of k . The final estimate here is then that ϵ_k has the same value for all of the longer wavelengths. At the largest spatial scale, L , we assume a typical velocity U and find

$$u_k = (\epsilon k)^{-1/3} = U(kL)^{-1/3} \quad (1.14)$$

This result holds until the dissipation is of the same order as the flux. Which then arises when

$$\epsilon \sim \nu(ku_k)^2 \quad (1.15)$$

Which then occurs when

$$k = k_D = L^{-1}(Re)^{3/4} \quad (1.16)$$

Here Re is the Reynolds number

$$Re = UL/\nu \quad (1.17)$$

Now, we can apply the scaling result to the power spectrum. Imagine that we move rapidly through the fluid and measure the velocity as a function of time, $u(t)$. Our speed V is much greater than any turbulent velocities. Then a fluctuation with wavelength k will appear us to be a fluctuation with frequency $\omega = kV$. The power we measure is the size of fluctuations with this frequency $u\omega/V$ squared times the typical time interval over which these fluctuations will be visible, ω^{-1} . Thus, we estimate

$$P(\omega) \sim \omega^{-1}(u\omega/V)^2 \quad (1.18)$$

From equation (1.14), we get

$$P(\omega) \sim \omega^{-1}U^2(\omega L/V)^{-2/3} \quad (1.19)$$

Equation (1.19) will apply until the frequencies get high enough so that dissipative effect will be come important. This will arises when k is or the order of the k_D estimated above. Then, to take care of this region of wave vectors we will need another factor $p^*(k/k_D)$ to represent the loss of power via dissipation. When this factor is inserted into Eq. (1.19), we get the scaling estimate

$$P(\omega) \sim \omega^{-1}U^2(\omega L/V)^{-2/3}p^*(\omega L(Re)^{-3/4}/V) \quad (1.20)$$

This is the estimate which was used for comparison with experiment.

I-4. Central Limit Theorem

I give one final example of simple scaling. Let X be a sum of N weakly correlated random variables x_j :

$$X = \sum_{j=1}^N x_j$$

According to the central limit theorem, under very general conditions, there is a simple form for the probability of observing X with the value X in the limit $N \rightarrow \infty$. The result is

$$\rho(X, N) = \text{const} \times N^{-1/2} \times \exp[-a[X - \langle X \rangle]^2/N]$$

Notice that the result is universal in the sense that it always has the same form independent of the probability distribution for the individual x_j . In fact, universality is characteristic of many scaling results. In the critical phenomena example, the function m^* is experimentally known to be the same for many different forms of the interactions among the basic entities. It varies almost only when the symmetry of the underlying phenomenon changes.

II. SOME THEORY

II-1. Binomial Distribution

Q objects are distributed randomly between 2 bins. The probability that P will be in bin 1 is

$$\rho(P|Q) = \frac{Q!}{P!(Q-P)!2^Q} \quad (2.1)$$

For large Q , the most likely result is that about half the objects will appear in bin 1. In fact, if we ask what is the probability that P will differ from $Q/2$ by an amount which is not too large, we once again get the central limit theorem result

$$\rho(P|Q) = (2\pi Q)^{-1/2} \times \exp[-[P - Q/2]^2/2Q] \quad (2.2)$$

However, we can also ask about large deviation of P from $Q/2$. These large deviations are very unlikely, but one can estimate their probability by using the Sterling approximation for the factorials

$$N! \sim \frac{N^N e^{-N}}{(2\pi N)^{1/2}} \quad (2.3)$$

which applies for large N . Then for large P and Q , the distribution (2.1) becomes

$$\rho(P|Q) = \text{const} \times Q^{-1/2} \times \exp[-Qf(P/Q)] \quad (2.4)$$

The major point is that the large parameter Q appears in the exponential multiplying a function of a quantity $a = P/Q$ which is of order unity. In this case

$$f(\alpha) = -\ln 2 - \alpha \ln \alpha - (1 - \alpha) \ln(1 - \alpha) \quad (2.5)$$

Near the peak (at $a = 1/2$) the distribution is Gaussian, but this result also works far into the wings.

We have here a very general result: Unlikely events are given by exponential distributions in which large parameters appear in the exponents multiplying functions which are of order unity.

II-2. A Little Bit of Theory

I would now like to derive a general form of distributions which look like the probability we got for the binomial case. The result in the binomial case can be written as

$$\rho(P|Q) \sim (e^{-Q})^{f(\alpha)} \quad (2.6)$$

Here we are saying that $\exp(-Q)$ is the small parameter in the problem and that we are raising the small parameter to a power. The power, $f(a)$, is of course a scaling index. The characteristic and special feature of this result is that in this case the power is not a constant but instead a continuously varying function of a . In some sense this is a problem in which there are an infinite number of critical indices. Since there are many critical indices this way of thinking is called a multi-scaling or (multifractal) approach.

Let us generalize this approach. Consider some conditional probability $\rho(X|L)$ where X , L are large numbers. (Here L is like our previous e^P and x is like our previous e^Q .) In a simple scaling approach one might say that ρ scales as the $-\nu$ power of L and X scales as the μ power of L . Then one would get a Widom-like form:

$$\rho(X|L) = L^{-\nu} \rho^*(X/L^\mu) \quad (2.7)$$

But now we generalize this formula to the case in which there are many critical indices labeled by subscripts i . Then this formula will become

$$\rho(X|L) = \sum L^{-\nu_i} \rho_i^*(X/L^{\mu_i}) \quad (2.8)$$

Now we make some assumptions. Let us order the indices in such a fashion that μ_i, ν_i both increase with i and assume that the scaling functions have the order of magnitude behavior

$$\rho_i^*(X) \sim \begin{cases} 1 & \text{for } x \ll 1 \\ 1 & \text{for } x \sim 1 \\ 0 & \text{for } x \gg 1 \end{cases} \quad (2.9)$$

Now look at the structure of the sum. To get an order of magnitude estimate take $X \sim L^{\mu_j}$. Then by our assumptions the term with $i = j$ sum dominates the sum and to an order of mag-

nitude

$$\rho(X|L) \sim L^{-\nu_i} \quad (2.10)$$

Finally assume that there are an infinite number of terms in the sum. Then the sum can be replaced by an integral. Write instead of μ_i , a . Use a as the integration variable. Since ν_i depends upon i it is a function of a . Write this function as $f(a)$. Now one can write instead of (2.8), the multiscaling expression

$$\rho(X|L) = \int d\alpha L^{-f(\alpha)} \rho_\alpha^*(X/L^\alpha) \quad (2.11)$$

One can now obtain a result analogous to (2.10) in this new formalism. Assume that to an order of magnitude $X \sim L^\alpha$. Then just the same argument which led to (2.10) now gives

$$\rho(X|L) \sim L^{-f(\alpha)} \quad \text{with } \alpha = \ln X / \ln L \quad (2.12)$$

We can convert this result into a recipe. Take a system which we suspect is multifractal described by some large (or small) parameter like reduced temperature or Reynolds number. Call this parameter L . Let us measure a quantity which varies over a considerable range called X . To see if Eq. (2.12) is right plot \log probability divided by $\log L$ against $\log X$ divided by $\log L$. If all the results for different L 's fall on the same curve, one has a multifractal spectrum of critical indices.

Now we have all our formal apparatus developed³. We can turn to specific examples.

III. SPECIFIC EXAMPLES

III-1. Sand Slides

Bak Tang and Wiesenfeld⁴ invented a cute dynamical model which shows how richly complicated events can arise in a relatively simple dynamical system. Let model sand be added grain by grain to a model sandpile, built upon a regular d -dimensional lattice. A one-dimensional version of the model is shown in Fig. 3.1. To start the cascade, one grain of sand is added to one of the columns, picked at random. In between additions, there are cascades of events in which sand falls downhill in response to a too-large local slope of the pile. In the particular model depicted in Fig. 3.1, the sand falls over whenever the column in question stands more than two above its right-hand neighbor. In that case, two grains of sand 'fall over' and land on the two columns to the immediate right of the unstable site. If a grain of sand reaches the right-hand end of the system, it falls off and disappears from view. At any given time, all columns that can fall do so, simultaneously. Then, if any columns remain unstable, they fall and so on. Thus the system can sustain 'avalanches'. The cascade of events continues until no more columns are unstable. Then another grain of sand is added at random and the entire process begins once more.

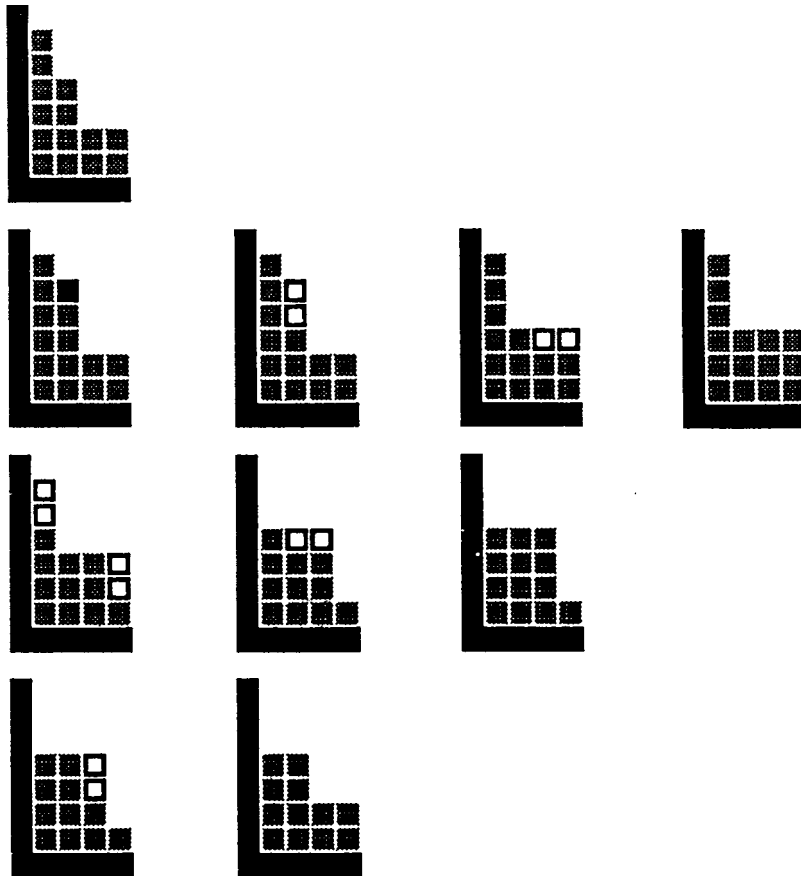


FIG. 3.1. The result of adding one grain of sand on the second column. The open boxes show the grains that fall.

The algorithm for the model is shown in the box below:

An Avalanche Model

Square Sand stacked up in a region of size L

A. Add a Grain at a Random Site

(Avalanche begins)

B. If the Slope (Height Difference) is greater than 2, two grains from stack fall over.

At right hand end, grains fall off

Continue until no more stacks are unstable.

(Avalanche Ends)

C. Return to A.

These avalanches in this system can be small or they can cover the entire system many times over. In our work⁶, we studied the nature of the probability distributions $\rho(X|L)$ for the probability that an event of size X will occur in a system with spatial extent L . We looked at two different quantities in some detail:

- a. The drop number D . In this case $X = D$ is the number of grains which fall of the end between two addition events.
- b. The flip number F . In this case X is the number of falling events which occur between two additions, and ask whether there is some scaling or universality. In low dimensions, $\rho(X,L)$ is most likely multifractal.

Like most of the examples discussed below, sands slides can be considered to be an example of self-organized criticality. That is, the system organizes itself in such a way that it is marginally stable against the occurrence of events within it. In this marginal stability, the system is just at the edge of stability. An event, once started, has a finite probability for growing larger at every stage of its early existence. It also has some probability for growing smaller and dying. These two probabilities balance out so that events of all sizes occur. In the sand pile. However, by the nature of the process $\rho(D|L)$ must have some weight for large D . In a large sandpile if the new grain falls far from the edge, the most likely events are sufficiently small so that the edge will never be reached and no grains will drop off. Hence, for $D = 0$, $\rho(D|L)$ is close to unity. For small D falling events will most likely occur only when the first grain falls near the edge. Hence they have a likelihood of order $1/L$

$$\rho(D|L) = c(D)/L \quad \text{for } D=1, 2, \dots \quad (3.0)$$

However, since the pile is in a kind of steady state, on the average one grain must fall for each grain added. In symbols

$$\sum_D \rho(D, L) D = \langle D \rangle = 1 \quad (3.2)$$

Eqs. (3.1) and (3.2) can only coexist if $\rho(D|L)$ has some weight for D of order L and hence non-trivial scaling structure. The same argument can be extended to show that the other probability functions, e.g. $\rho(F|L)$, also have non-trivial scaling structures. This is an indication that events which involve large values of D and F must play an important role in determining the steady state dynamics of avalanches.

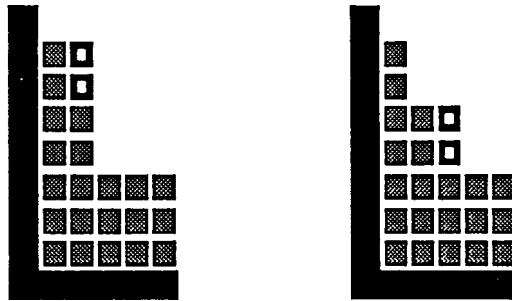
We want to know the answer to two questions:

- a. What kind of scaling occurs? Is it the simple scaling or is it a multifractal distribution? Perhaps it is something else altogether.
- b. How universal is the result. Do different sets of rules give the same answers?

To answer these questions, we turn to simulations of the flow in sandpiles.

Consider a variant of the model indicated in Fig. 3.1. We work with a one dimensional

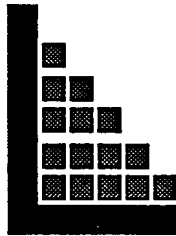
array of stacks of sand. (See Fig. 3.2) The cascade occurs when the height difference between neighboring stacks is higher than NF . For all stacks which satisfy this condition, then NF grains on sand will fall onto the right-hand neighboring stack. This process continues until the cascade ends.



LIMITED LOCAL $NF=2$

FIG. 3.2. One avalanche in the local limited $NF = 2$ model. The model is limited in the sense that if the slope is bigger than NF , still only NF grains will move. It is local in the sense that the grains all move to the next site to the right. (downhill).

The case with $NF = 1$ is trivial. The sandpile gets into a state where the slope is one everywhere. See Fig. 3.3. If a grain is added it just goes step by step to the right until it falls



$NF = 1$

FIG. 3.3. The case of $NF= 1$. The sandpile reaches a trivial configuration which the slope is one everywhere.

off the end. Thus, the probability distribution is trivial

$$\rho(D|L) = \delta_{D,1} \quad (3.3)$$

However, as soon as $NF = 2$, the situation becomes much more complex and interesting. Fig. 3.4a shows the probability distribution obtained from computer simulations for cases in which

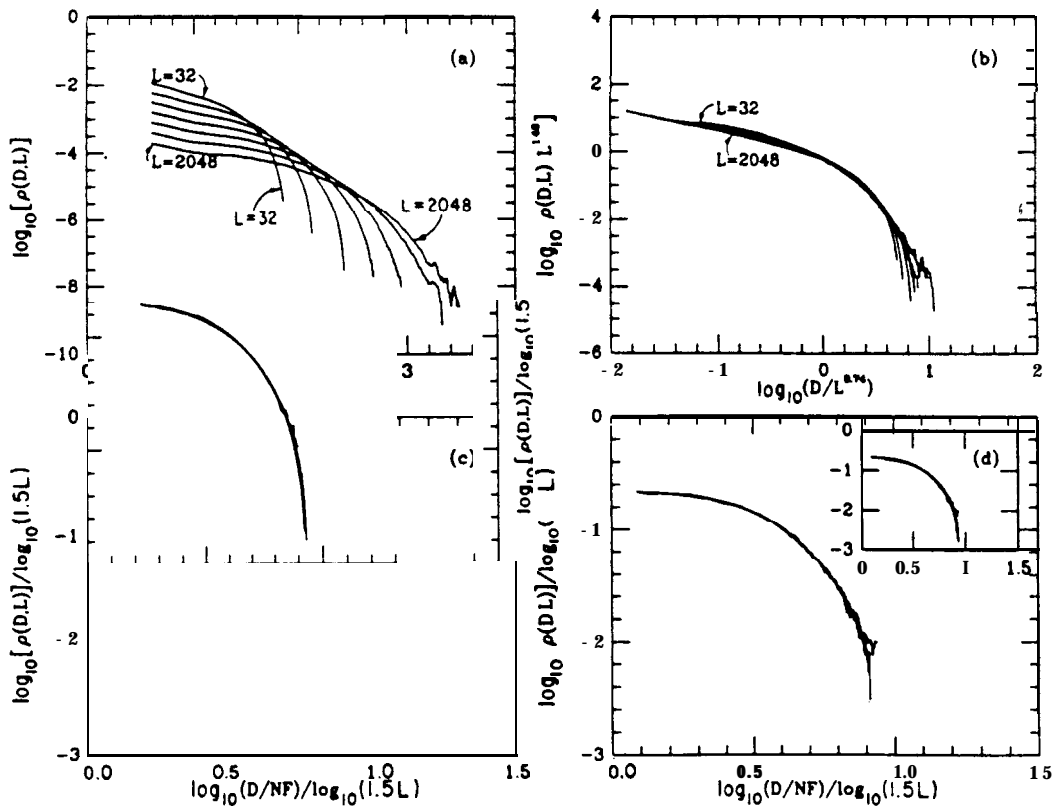


FIG. 3.4. (from Kadanoff, et al. see reference 6, Figure 1.) Distribution of drop number in a one dimensional model. Part a shows that raw data for $NF=2$. The system size, L , ranges from 32 to 2048. Part b shows the best scaling fit to these data. This fit is much worse than the multiscaling fit shown in part c. In part d, the same fit is shown for $NF=20$. The inset compares $Nf=2$ with $NF=20$, showing that the $f(a)$ is the same for both cases.

L varies from 32 to 2048. This figure is drawn for simulations in which $NF=2$. Notice the very wide distribution of probabilities. One can try a simple scaling analysis of the form

$$\rho(D|L) = L^{-p} G(D/L^q) \quad (3.4)$$

Figure 3.4b shows the best fit of this form which we were able to obtain. Notice that although the data is well-fit in the central region, the fit is not wonderful for either small D or large D . On the other hand we might try a multifractal fit in which logs of physical quantities are divided by logs of the large parameter in the problem. For this case the appropriate functional fit is to try

$$\frac{\log \rho(D|L)}{\log L} = f(\log D / \log L) \quad (3.5)$$

A slight improvement in the fit can be obtained by taking the measured quantities and multi-

plying by a constant and so using the fit

$$\frac{\log \rho(D|L)}{\log AL} = f(\log(BD)/\log AL) \quad (3.6)$$

Here we choose $A = 1.5$ and $B = 0.5$. The fit is good if when $\log \rho(D|L)/\log AL$ is plotted against $\log(BD)/\log AL$, a single curve is obtained. Fig. 3.4c shows a fit of this form for the data under consideration. The fit is excellent. We conclude that a multiscaling or multifractal analysis is the right one.

Notice incidentally that there is no way that the curves in Fig. 3.4 indicate that there is really simple scaling. If there were, the pictures would show a large straight line region representing power law behavior of $\rho(D|L)$. There is really no readily apparent single slope, or single power law.

Now we are in a position to ask another question. What is the range of applicability of the fit (3.5)? Is there some 'universal' behavior of large cascades. In particular, if we change the model somewhat will the answer (*viz* the form of the function f) change. Fig. (3.4c) shows the form of the function f for a different model, or rather for the same model with $NF = 20$. There is no trivial sense in which these models are identical. Nonetheless the forms of $f(\alpha)$ for the two models are, as far as one can tell, exactly the same. (See especially the inset in the figure in which the two f 's are superposed.)

In a more recent work⁷, O'Brien et al have considered what happens in higher dimensions. Perhaps, one might say, the multiscaling behavior which was apparent in one dimension does not apply for higher dimensions. Fig. 3.5 shows the analysis of three dimensional arrays of stacks for a model which is a simple generalization of the one described above. The net result is that once again the multiscaling analysis gives a better fit. There is in three dimensions, a somewhat longer region of power law behavior, which can be fit by either the simple scaling or the multifractal approach. However, at the right hand end of the curve, the multifractal analysis clearly wins the day. The right hand side of the curve represents large events in which many grains of sand do fall off the edge. These drop events reduce the number of grains of sand in the pile and eventually dissipate the avalanche. Apparently, this dissipation is well-represented by a multi-fractal analysis.

III-2. Convective Turbulence

Recent experiments by Albert Libchaber's group^{8,9} have shown how very beautiful and intricate structures may arise in situations in which one expects to observe hydrodynamic turbulence. The experiments in question involve a 'Rayleigh-Bénard' flow. In this flow, the fluid is set into motion by placing it in a box and heating it from below. The heated, and therefore less dense, fluid will rise. Correspondingly, the colder and less dense fluid will fall. The net effect that the whole fluid will move and carry heat from bottom to top.

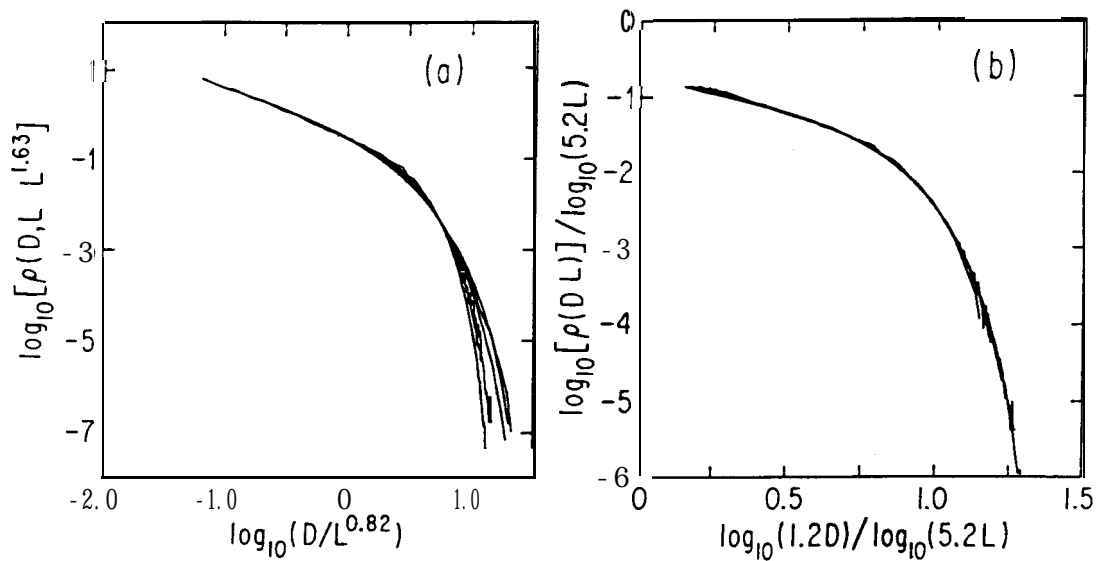


FIG. 3.5. (Taken from O'Brien et al. (see ref. 7, Fig. 2.)) The same as the previous figure but for the **three-dimensional** model. The left-hand plot shows the best simple scaling fit that the authors could obtain. The right hand plot shows the multifractal fit. The latter is much better.

There is a dimensionless number which describes the strength of the forcing in this type of experiment. It is called the **Rayleigh** number and is given by

$$Ra = \frac{g\alpha\Delta L^3}{\kappa\nu} \quad (3.7)$$

Here, g is the acceleration of gravity, α is the volume thermal expansion coefficient, Δ is the temperature difference between the bottom and the top of the cell, κ and ν are respective the thermal diffusivity and the kinematic viscosity, and L is a characteristic size of the cell. More physically, $g\alpha\Delta$ is a typical size of the buoyant forces which are trying to get fluid into motion while κ and ν are measures of the contrary forces which are working to put the system into equilibrium. High values of Ra correspond to large forcings and indicate a situation in which the fluid is likely to be highly turbulent. The turbulence is easily seen for example (see reference 23) in a setup in which the working fluid is water in a rectangular tank with typical dimension about 20 cm and typical temperature difference Δ about 10 degrees centigrade. In that case, one can see a very chaotic pattern of motion within the tank. Measurements on an analogous system composed of low-temperature helium gas, where there is a better possibility for accurate measurement but a worse possibility for visualization, show scaling types of behavior roughly

analogous to the ones discussed above. The environment is certainly very noisy and the measurements show many elements of randomness.

We turn our attention to the part of the experiment which measures the temperature as a function of time in the center of the cell." In this region, we are seeing quite well-developed turbulence. In fact, since the strongest shears are toward the side walls of the container, perhaps it is appropriate to say that what is looking at is the decay in space and time of well-developed turbulence. The quantity under examination is the power spectrum, the squared magnitude of the fourier transform of temperature as a function of time.

The basic data¹¹ for one cell is shown in Fig. 3.6. In the spirit of the usual scaling analysis

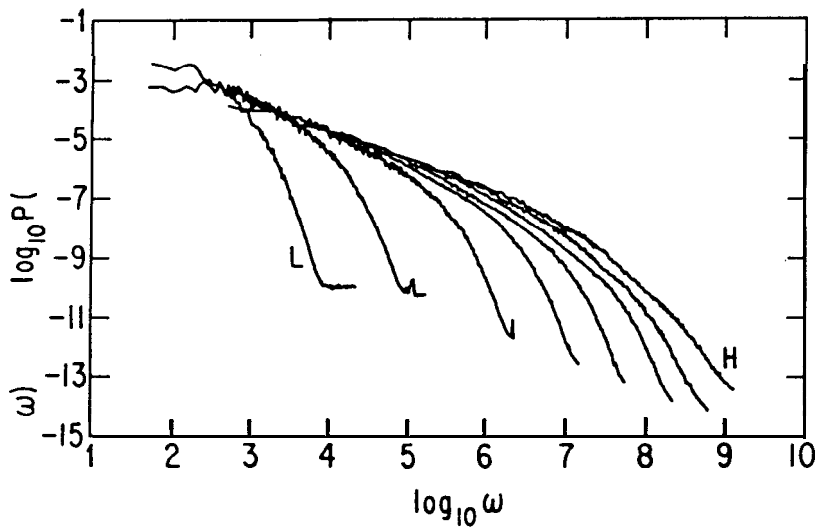


FIG. 3.6. The experimental data. Power, P , is plotted as a function of angular frequency, ω . Taken from ref. 10. The symbol H marks the highest frequency, L the lowest.

we try to fit the data by considering $P(\omega)$ to be of the form:

$$\ln P(\omega)/P_h(Ra) = F(\ln \omega/\omega_h(Ra)) \quad (3.8)$$

Here we take P_h and ω_h to be adjustable constants, which we try to fit for each data set (value of Ra) so that all the data in Fig. 3.6 falls upon a single curve. We show such a scaling fit in Fig. 3.7. This figure includes all the samples for lower values of the Rayleigh number, $10^7 < Ra < 7 \times 10^{10}$. As one can see, in the central region of frequency this scaling fit is extremely good. Hence, we do have a region in which simple scaling works. The failure of the fit at high frequencies is an experimental artifact due to the finite resolution of the thermometer. The low frequency failure is a different story. There is a characteristic frequency, ω_p , which represents

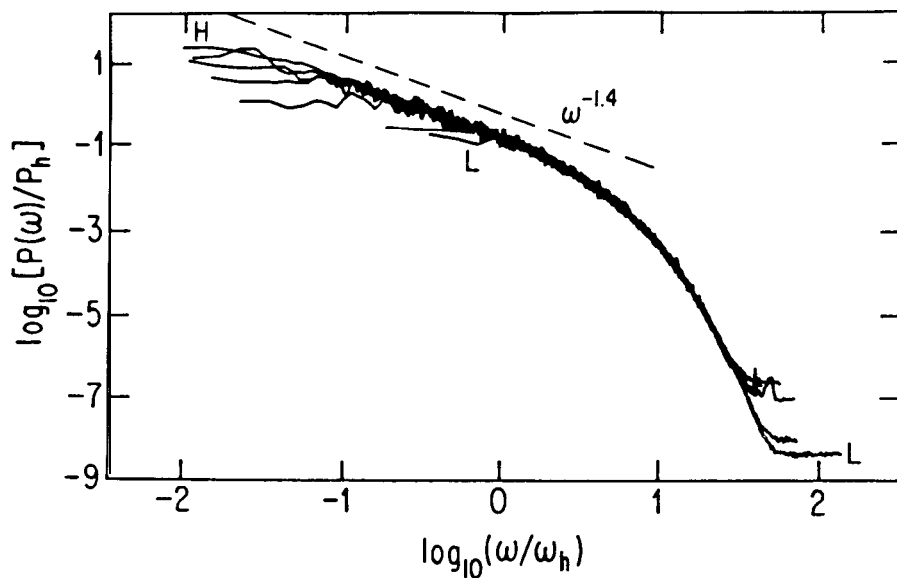


FIG. 3.7. The experimental data normalized so that it fits upon a single curve. Taken from ref. 10. The normalizing factors, P_h and ω_h depend upon Rayleigh number. The data shown here includes all cases where $Ra < 7 \times 10^{10}$. The symbol H marks the highest frequency, L the lowest.

a typical frequency for the overall flow around the cell. It is in fact, a typical transit time for a revolution of the liquid around the cell. The physics of this large-scale effect does not fit into the scaling picture. Hence the failure of the scaling fit a low frequencies. As Ra gets larger and larger, in this region, the fit works over a large region of dimensionless frequency.

Notice the straight line region of the plot. This is a result of the region in which there is a Kolmogorov style cascade, and in which the dissipative effects have not yet become important. (They only become important at higher frequencies.) In this region we have that the power goes as ω raised to the -1.4 power. Thus our general fit is of the form¹²

$$P(\omega) \sim \omega^{-7/5} \times p^*(\omega/\omega_h(Ra)) \quad (3.9)$$

Equation (3.9) fails for higher values of Ra . Hence, we try a multifractal fit, one of the form

$$\frac{\ln P(\omega)/P^*}{SF(Ra)} = \frac{F(\ln \omega/\omega^*)}{SF(Ra)} \quad (3.10)$$

In the spirit for multifractal analysis, we have taken the log log representation of our data and compressed the data by using a scale factor which depends upon Ra . In doing this, we have the other normalizing factors (now called P^* and ω^*) and taken them to be independent of Ra . The scaling factor, SF , is taken to be of the form

$$SF(Ra) = A + B \ln Ra \quad (3.11)$$

Figure (3.8) shows a plot of the appropriate range of the data, $7 \times 10^{10} < Ra < 7 \times 10^{14}$, using the data correlation of Eq. (3.10). If this equation is right, all the data should fall on a single curve. Once again, in the central regions of frequency, the fit works in an excellent fashion. The failures for higher and lower frequency are explained as before.

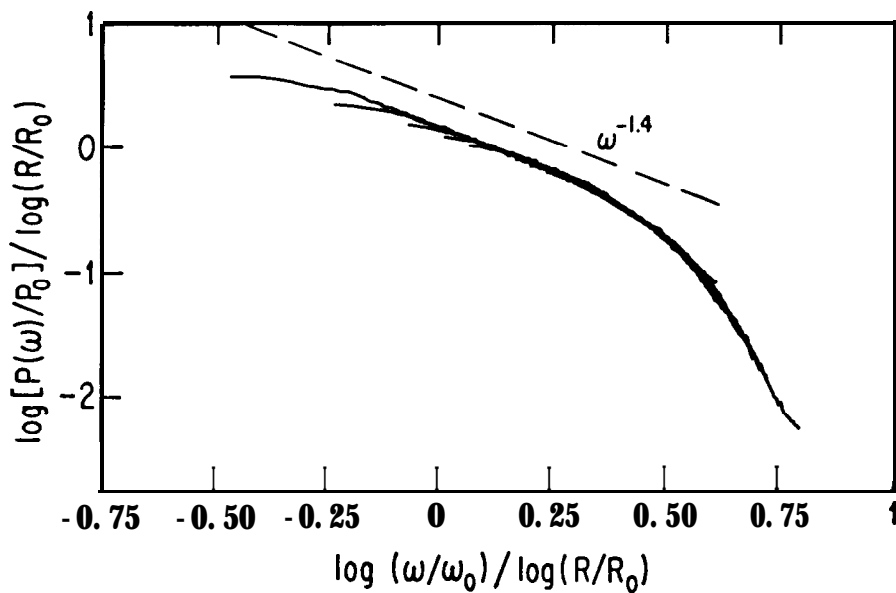


FIG. 3.8. The high **Rayleigh** number experimental data with the logarithmic scales normalized so that the data fits upon a single curve. Taken from ref. 10. The normalizing factors, P_0 and ω_0 and R_0 do not depend upon **Rayleigh** number. The data shown here includes all cases where $Ra > 7 \times 10^{10}$. The symbol H marks the highest frequency, L the lowest.

Equation (3.9) suggests that there is a characteristic critical index (≈ -1.4) associated with the power spectrum. If the plot in Fig. 3.8 had straight-line regions, each of those regions would have a slope which is a critical index for the data. However, there is no substantially large straight-line region except perhaps the one at the lower end of the fit frequencies. Therefore, one says once more that there is a whole spectrum of critical indices which describe the data.

Because the data set for $Ra = 7 \times 10^{10}$ falls in both the scaling and the multiscaling plots, one single curve with one value of F will fit all the data. The general fit is of the form

$$\frac{\ln P(\omega)/P_h}{SF} = \frac{F(\ln \omega/\omega_h)}{SF} \quad (3.12)$$

Here, for $Ra < 7 \times 10^{10}$, the scaled factor, SF, is independent of Ra while for $Ra > 7 \times 10^{10}$, P_h and ω_h are independent of Ra. The very same F describes all data.

III-3. Glasses

The work of Dixon, Wu, Nagel, Williams, and Carini¹³ has led to the surprising result that dielectric relaxation in glasses can also be described by a variant of a multifractal analysis. Glasses relax slowly to equilibrium. The lower the temperature, the slower the relaxation. Of course, this slowness is the reason why we can use a liquid, window glass, in our buildings and have the windows remain in place for many centuries. After a while, they will flow downward and form a puddle.

This discussion assume that as the temperature is lowered, but the material remains glassy, there is never a true phase transition to a qualitatively different state of matter. If the phase transition occurs at some temperature or another, below this temperature there will emerge a qualitatively different form of the behavior of the material. Hence by examining the form of the dielectric relaxation in the results of Dixon et. al., one can see whether a phase transition does indeed occur. As we shall see, there is never an apparent change in behavior. Thus, within the experimental range, the phase transition appears to be ruled out.

This slowness of the relaxation can be studied by looking at the frequency dependent of the dielectric 'constant', $\epsilon''(\nu)$. Fig. (3.9) shows the imaginary part of the dielectric function

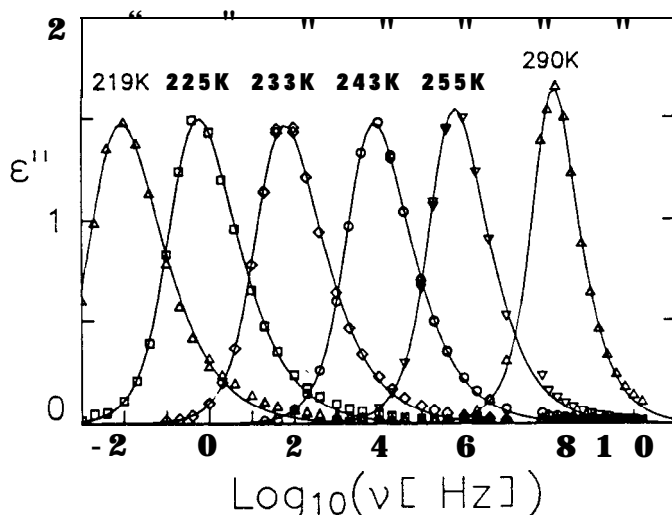


FIG. 3.9. Figure 2b of Dixon et al (ref. 12). The imaginary part of the dielectric constant, ϵ'' , plotted against frequency, ν , for various temperatures. The data seems to be well fit by a stretched exponential form as shown by the solid lines. However, this form does not work well in the tails.

plotted as a function of frequency, here called ν . The characteristic microscopic frequency is 10^{13} or so Hertz. The typical frequencies seen in this glass, salol, range from 10^9 Hertz to 10^{-2} Hertz for the temperature range shown here. The solid curves are fits to the data obtained from a stretched exponential form of fit

$$\varepsilon''(\nu) = -\ln[\text{fourier transform of } (\frac{d}{dt}\exp(-|\nu_p t|^\beta))] \quad (3.13)$$

Here β and ν_p are taken to be adjustable function of temperature. As the data is presented in Fig. (3.9), the stretched exponential seems to fit just fine. However, if one looks in the tail of the data the fit of Eq. (3.13) fails by up to a factor of thirty or so. However, one can make use of the structural form of Eq. (3.13) to get an excellent fit to the glassy relaxation data. Eq. (3.13) implies that

$$\frac{\log(\varepsilon''(\nu)\nu_p/(\nu\Delta\varepsilon))}{w} = F\left(\left(1 + w^{-1}\right)\frac{\log \nu/\nu_p}{w}\right) \quad (3.14)$$

Here $\Delta\varepsilon$ is a fitted normalization factor. The other fitting parameter, w^{-1} , is of the order of β . It is taken to be the half-width of the ε'' curves. There is a particular form of $F(a)$ which goes with the stretched exponential. Notice that Eq. (3.14) is, except for one small difference, exactly of the same form which we have used heretofore. In a log log representation, physical quantities are divided by scaling parameters, here w , which depends upon the key control parameter, here temperature. The only difference is that here there is an extra factor $(1 + w^{-1})$ which has no analog in our previous fits.

Despite this 'imperfection', the authors of this paper used Eq. (3.13) because it gave an excellent way of representing their data. For each material and each temperature, they fitted a value of w and of $\Delta\varepsilon$ and then plotted the data in the form suggested by Eq. (3.14). The result for salol (and all the data shown in Fig. 3.9) is given in Fig. 3.10a. Each data point fits beautifully on one smooth curve. Fig. 3.10b shows the same plot with many different glasses superposed. Apparently, in this representation, the glassy data is universal. Furthermore, it cannot be fit by a stretched exponential. Fig. 3.10c shows the best stretched exponential fit to the data in glycerol. The simple fit clearly fails for the higher frequencies.¹⁴ Furthermore, the stretched exponential does not work at lower frequencies either since for $\nu \sim \nu_p$, the Fourier transform of the stretched exponential agrees with neither Eq. (3.14) nor the experimental data.

Once again the straight line of the simple fit describes a single critical exponent, here β . Once again, the single exponent fails to fit the data but the multiscaling fit, which uses many exponents, does work. Clearly there is some magic in these fits. But what does it all mean?

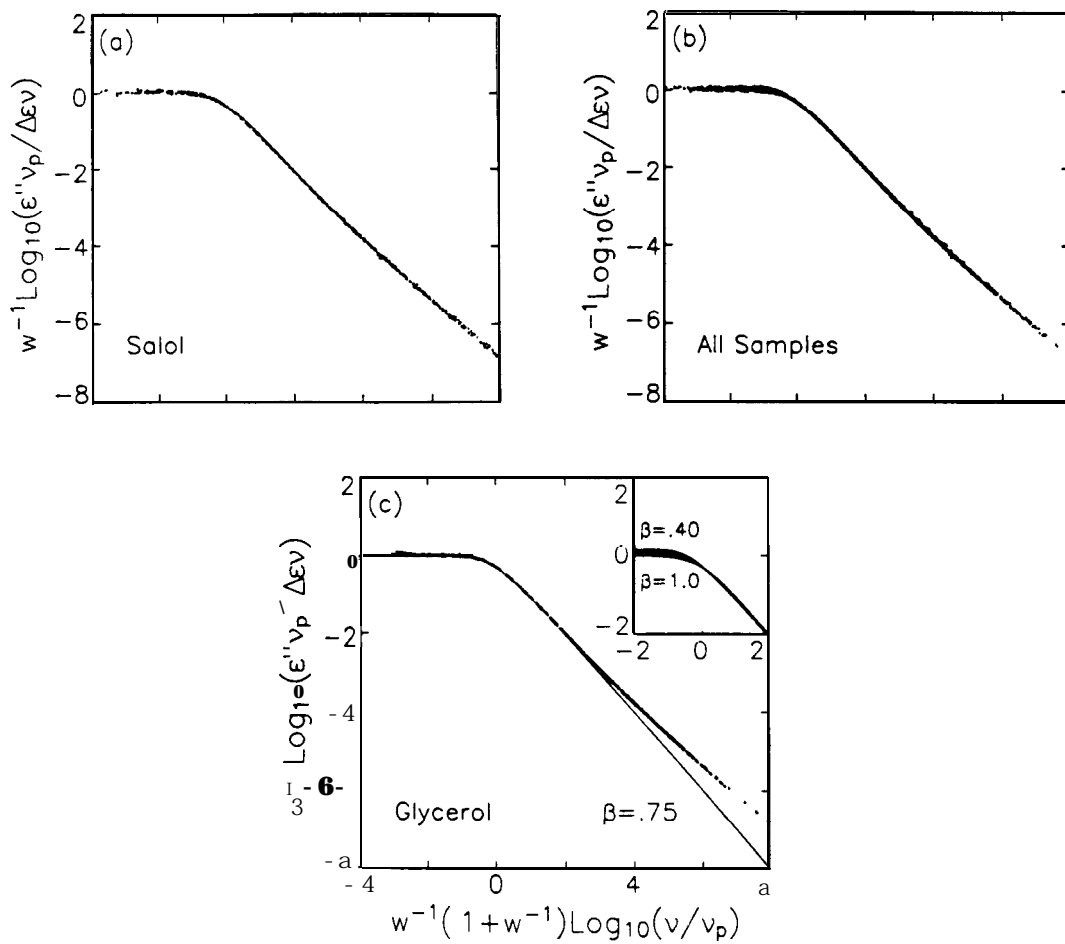


FIG. 3.10. Drawn from Fig. 3 of Dixon et al (ref. 13). The first part shows the same data as in Fig. 3.9, but now in a log log plot. The result plotted in this way is temperature independent. Part b shows the data for the seven different glasses studied in this reference. Note that they all fall onto the same curve. The third plot shows the data for the glassy material, glycerol. The line is the best stretched exponential fit. Notice that this 'best fit' is not too good. Nonetheless the multifractal fit gives an excellent result.

REFERENCES

1. The description in Radu Balescu, "Equilibrium and Nonequilibrium Statistical Mechanics", Wiley (1975).
2. A. S. Monin and A. M. Yaglom, "Statistical Fluid Mechanics", The MIT Press.
3. This 'multifractal' analysis was well known in the mathematical literature as a method for studying low-probability events. In more physical contexts, it was introduced by Mandelbrot J.

- Fluid Mech.* **62**, 331 (1974). For the study of turbulence and then further applied by U. Frisch and G. Parisi in *Turbulence and Predictability in Geophysical Fluid Dynamics and Climate Dynamics*, edited by M. Ghil, R. Benzi and G. Parisi (North-Holland, Amsterdam, 1985) p. 84. See T. Halsey, M. H. Jensen, L. Kadanoff, I. Procaccia, and B. Shraiman *Phys. Rev.* **A33**, 1141 (1986), For an exposition of this thinking.
4. P. Bak, C. Tang and K. Wiesenfeld, *Phys. Rev. Lett.* **59**, 381 (1987); P. Bak, C. Tang and K. Wiesenfeld, *Phys. Rev.* **A38**, 364 (1988).
 5. Real sand does not behave in precisely the same manner as model sand. See H. M. Jaeger, Chu-heng Liu and Sidney R. Nagel, *Phys. Rev. Lett.* **62**, 40 (1989), but also G. A. Held, D. H. Solina II, D. T. Keane, W. J. Haag, P. M. Horn and G. Grinstein IBM Yorktown Heights preprint (1990).
 6. Leo Kadanoff, Sidney Nagel, Lei Wu and Su-Min Zhou, *Phys Rev.* **A39**, 6524 (1989).
 7. Kevin O' Brien, Lei Wu, and Sidney R. Nagel, " Avalanches in Three and Four Dimensions" , University of Chicago preprint, 1990.
 8. Giovanni Zocchi, Elisha Moses, and Albert Libchaber *Physica A***166**, 387 (1990).
 9. S. Gross, G. Zocchi and A. Libchaber *Compt. Rend, Acad Sci (Paris)* 307 (1988). E. Moses, G. Zocchi, I. Procaccia, and A. Ubchaber (preprint 1990).
 10. A longer description of the experiment and of the scaling analysis of it appears in B. Castaing, G. Gunaratne, F. Heslot, L. Kadanoff, A. Libchaber, S. Thomae, Xiao-Zhong Wu, S. Zaleski and G. Zanetti, *J. Fluid Mechanics*, **204**, 1 (1989).
 11. This work is described in Xiao-Zhong Wu, Leo Kadanoff, Albert Libchaber, and Masaki Sano, *Phys. Rev. Letts Phys. Rev. Letts* **64**, 2140 (1990).
 12. The $7/5$ is the power law expected for convective systems. See V. Lvov, Weizman Institute preprint (1990).
 13. Paul Dixon, Lei Wu, Sidney Nagel, Bruce Williams, and John Carini, " Scaling in the Relaxation of Supercooled Liquids" , University of Chicago preprint, 1990.
 14. Equation (3.14) fits the high frequency data (that for $\nu > \nu_p$) quite well. However, at lower frequencies, it appears that some additional physics enters, and the universal multifractal fit fails.